Chapter 13
Learning Fast Hand Pose Recognition

Eyal Krupka, Alon Vinnikov, Ben Klein, Aharon Bar-Hillel, Daniel Freedman, Simon Stachniak and Cem Keskin

Abstract Practical real-time hand pose recognition requires a classifier of high accuracy, running in a few millisecond speed. We present a novel classifier architecture, the *Discriminative Ferns Ensemble* (*DFE*), for addressing this challenge. The classifier architecture optimizes both classification speed and accuracy when a large training set is available. Speed is obtained using simple binary features and direct indexing into a set of tables, and accuracy by using a large capacity model and careful discriminative optimization. The proposed framework is applied to the problem of hand pose recognition in depth and infrared images, using a very large training set. Both the accuracy and the classification time obtained are considerably superior to relevant competing methods, allowing one to reach accuracy targets with runtime orders of magnitude faster than the competition. We show empirically that using DFE, we can significantly reduce classification time by increasing training sample size for a fixed target accuracy. Finally, scalability to a large number of classes is tested using a synthetically generated data set of 81 classes.

E. Krupka · A. Vinnikov · B. Klein · A. B. Hillel (✉) · D. Freedman
Microsoft Research, Herzelia, Israel
e-mail: aharonb@microsoft.com

E. Krupka
e-mail: eyalk@microsoft.com

A. Vinnikov
e-mail: t-alvinn@microsoft.com

B. Klein
e-mail: t-benk@microsoft.com

D. Freedman
e-mail: danifree@microsoft.com

S. Stachniak
Microsoft Console dev R&D, Redmond, WA, USA
e-mail: szimons@microsoft.com

C. Keskin
Microsoft Research Cambridge, Cambridge, UK
e-mail: cemke@microsoft.com

L. Shao et al. (eds.), *Computer Vision and Machine Learning with RGB-D Sensors*,
Advances in Computer Vision and Pattern Recognition,
DOI: 10.1007/978-3-319-08651-4_13

13.1 Introduction

The trade-off of speed versus accuracy is an important topic, widely discussed in the object detection and recognition literature [3, 7, 11, 19, 25]. In applications like Natural User Interface (NUI), algorithms have to obtain high recognition accuracy in real time, on low power platforms. Often accuracy must be obtained with only a small fraction of the available CPU resources, reserving CPU cycles for other operations. The trade-off is natural: high accuracy requires a rich representation, with considerable computational cost at all levels of the system. At the lowest level, this includes using dense sampling of complex local descriptors [21, 27]. Further on, multiple spatial aggregation layers are employed [6, 18], with large dictionaries at higher levels. At the highest level, the best accuracy is often obtained using non-linear kernels [6, 18], requiring kernel computation with many support vectors.

In this section, we attack the problem of hand pose classification using infrared (IR) and depth images from a time of flight depth camera, in the context of a NUI application. There are dual demands for high accuracy and a very low computation budget, the latter a fraction of a millisecond on a low-end CPU. For our problem, standard techniques achieved reasonable enough accuracy for a moderate training set size, but were unable to meet the classification time requirement. One can improve speed by modifying the parameters of such techniques; for example, one may reduce grid density or dictionary size. However, experiments show that this approach is limited, when the target speed is obtained accuracy drops too much.

This calls for a wider consideration of recognition systems based on machine learning. Beyond accuracy and speed, these systems have additional performance characteristics: generalization ability (i.e., ability to learn from a relatively small training set size), training time, and memory consumption. Suppose that it is possible to collect a very large training set, there is no significant limitation on training time, and a moderate amount of memory is available at test time. The question then becomes: for a fixed accuracy target, can we trade training set size for increased speed at test time?

The algorithm proposed here pushes the speed–accuracy envelope at the expense of larger training sets using three steps. First, simple non-invariant features are used, with sharp non-linearity, as they are fast to compute. Using a large enough training set, we can hope that the task-relevant invariance will be learned instead of *a priori* encoded. Second, and most important, an architecture with large capacity and minimal computation is introduced, based on an ensemble of large tables encoding the end results. Such table-based classifiers, termed 'ferns' [6, 19, 24], have high capacity with a VC-dimension higher than 2^K for a single 2^K-entry table, and close to $M2^K$ for a M-tables ensemble.[1] Third, since the classifier form presents a hard learning problem, with high capacity and minimal prior, we develop a discriminative optimization framework for a fern ensemble, which is a departure from the generative formulation used previously for ferns.

[1] Assuming that the underlying space is of dimension higher than K and MK, respectively, which are satisfied for the image sizes considered.

Focusing on speed optimization, we use as features spatial aggregates of highly simplistic features, i.e., pixel-pair comparisons; A set (ensemble) of lookup tables (ferns) are then built based on sets of such bit features. Each fern is based on a set of K simple binary features and a large table of 2^K-entries. The binary features are concatenated into an index, and the corresponding index entry in the table contains a weight contribution, summed across the ferns to get the final classification. Each table can be regarded as an efficient codeword dictionary: It maps a patch into one of 2^K words, yet at the cost of K operations. The resulting architecture is highly non-linear, and a feed-forward push of an image through it only requires multiple bit computations and table access operations.

Ferns are traditionally formulated generatively, i.e., conditional class probabilities are stored at the table entries. In contrast, we suggest training the ensemble discriminatively by minimizing the regularized hinge loss, i.e., the loss minimized by Support Vector Machines (SVM). The minimization technique is related to ideas from the Predictive Feature Selection (PFS) algorithm [2]. It is done agglomeratively in a boosting-like framework, promoting complementariness between chosen ferns and between bits in a single fern.

The main technical contribution of this section is in the introduction of a *Discriminative Ferns Ensemble* (*DFE*) approach and empirically demonstrating its ability to considerably shift the speed–accuracy curve. The method is applied to hand pose recognition from IR and depth images, and compared to the best alternatives for this task. In this comparison, the DFE achieves accuracy comparable or better while being one to two orders of magnitude faster. In particular, it is significantly more accurate than a classification based on deep random trees, which have been used for similar tasks [17, 25] and considerably more accurate than a more standard ensemble of random ferns [6, 24]. Several general object recognition methods were also applied to the task, combining fast dense SIFT features, DAISY, random forest dictionaries, and SVM [23, 29, 30]. The best results achieved were slightly less accurate than DFE, but classification time was two orders of magnitude (i.e., 100 times) slower. DFE is also shown to be efficient when the number of classes increases, utilizing ferns sharing between classes and an error-correcting output code (ECOC) classification methodology minimizing the number of classifiers trained.

A second contribution is that we empirically show significant improvements in classification speed—for a given target accuracy—can be achieved by collecting larger training sets. This is done by optimizing K (log of the table size) and M (number of ferns) for a given training set size. In other words, if a DFE classifier is accurate, but not fast enough, collecting larger training set can be used to accelerate classification speed. Note that this trade-off is different from the well-known trade-off between training set size and accuracy.

The approach presented was found practical and was used to train the hand pose recognition in XBox-1, shipped in early 2014.

We discuss related work in Sect. 13.2 and present our approach in Sect. 13.3. In Sect. 13.4, we summarize a set of experiments in which ingredients of the method are tested and the approach is compared with competing techniques. We briefly conclude in Sect. 13.5.

13.2 Relevant Work

With the emergence of cheap $3D$ sensors, and primarily the Kinect sensor, pose estimation and recognition in IR+depth images have been the subjects of increasing study in recent years [1, 5, 10, 15–17, 20, 25, 26]. In contrast to working with RGB images, the depth information enables easier segmentation of body parts, simpler reasoning about occlusion, and usage of simpler features enabling real-time applications. We focus here on techniques that have been applied to hand pose recognition and estimation, as well as more general techniques that bear some similarity to the proposed DFE method.

An important line of work that has influenced our technique uses random forests as the main tool, with the notably successful application of this technique to body pose estimation in the Xbox-360 [25]. In [16], a random forest is trained to classify pixels according to hand part labels. The hand parts positions are then estimated by finding the mode of the posterior part probability using mean shift. In [17], this method is extended to a two-stage method. In a preprocessing stage, the pose space is clustered into 50 clusters, corresponding to global hand shapes. A first random forest is trained to classify pixels as belonging to images from one of the 50 clusters. In the second layer, 50 different random forest 'experts' are trained, one for each of the clusters. Part position estimation is performed by using the chosen expert from the second layer, or by splitting decisions regarding pixels among their most plausible 'experts.' Good empirical results are reported for shape classification (using the first stage) and for pixel part classification.

The pose estimators mentioned above were trained using large datasets of synthetic data, but the random forest-based approach was extended to include a mixture of labeled real data, unlabeled real data, and synthetic data in [26]. The forests trained in this approach included mixed regression and classification trees, and several criteria for node splitting were combined, including a criterion requiring low variance and a criterion requiring that real labeled data and synthetic data with the same label share the same node.

While the random forest approach usually relies on very simple features, another line of work focuses on learning more complex features integrating RGB and depth information. The methods suggested in [1, 5] learn hierarchical descriptors that aggregate RGB and depth information across increasingly larger spatial area. Both show significant improvements in general object recognition using descriptor level fusion of RGB and depth. In [20], an approach is presented, which learns spatio-temporal complex features for a difficult gesture recognition task. Increasingly complex features are created by composition of basic operators like filtering, spatial averaging, and non-linear operations. A genetic algorithm is used to choose the most discriminative features for a linear SVM classifier.

A different traditionally popular approach poses hand pose recognition as a retrieval problem [10, 13]. In [10], a large dataset of synthetic images with known pose parameters was created. The hand is carefully segmented (Kinect depth images are used) and compared to database images using several distance functions: Chamfer distance, L^2 distance between the depth images, and a combination of the two.

Empirical results show that the correct match is often ranked high in the list of retrieved images.

As stated above, fast recognition methods are often based on trees or ferns ensembles [6, 9, 12, 17, 24, 25]. Ferns are often regarded as a special case of trees, in which the condition encoded at all the nodes with the same depth is identical. Boosting of decision trees is a highly popular technique for object detection and classification in RGB [9, 12], but usually shallow trees of depth 1–3 are used, which cannot capture fine-grained partitions. Ferns ensembles were suggested in recent years for RGB image classification [6], keypoint recognition [24], and nearest neighbor finding [19]. In these works, ferns in the ensemble are chosen independently of each other, and bits in a single fern are chosen at random or using an information gain criterion. At the leaves, conditional class posteriors are computed and averaged across ferns [6], or regulated with a prior and multiplied [24].

Among the tree-based methods mentioned above, the works presented in [16, 17, 25] are most related to the DFE, as they also allow fast, real-time classification using simple pixel comparison features and a tree ensemble architecture. However, the DFE departs significantly from the random forest and random ferns tradition in its resort to discriminative optimization. In a DFE, the fern ensemble is regarded as providing the features for a large L_2-SVM problem. Ferns and bits are not chosen at random, nor using a general information criterion, but picked to minimize the loss of this program. In particular, the gradient of the SVM program with respect to adding new features is computed at each round and used to guide choice of the bits in the new fern. Ferns (and bits) are hence grown to be complementary, as in a gradient boosting process [22]. The weights of the fern's table, corresponding to the leaves of a tree, are not conditional probabilities, but rather SVM weights. Due to this optimization, a DFE is more accurate, requires less memory, and less CPU time than approaches presented in [16, 17, 25]. We discuss the differences in Sect. 13.3.2 and compare the methods empirically in Sect. 13.4.

13.3 The Discriminative Ferns Ensemble

We describe the Fern Ensemble classifier in Sect. 13.3.1 and analyze its running time in Sect. 13.3.2. In Sect. 13.3.3, we present the training procedure we use.

13.3.1 The Discriminative Ferns Ensemble Classifier

The ferns ensemble classifier operates on an image patch, which we denote by I, consisting of P pixels. For a pixel p, we denote its neighborhood by $N(p)$, and we denote by $I_{N(p)}$ the subpatch which is comprised of the pixels in p's neighborhood. In what follows, we will consider $I_{N(p)}$ as a vector in $\mathbb{R}^{|N(p)|}$. The ferns ensemble consists of M individual ferns, and its pipeline includes three layers whose structure we now describe.

Bit Vector Computation Let us focus on one particular fern m. For each pixel p, we compute a local descriptor of its neighborhood subpatch $I_{N(p)}$ using computationally light pairwise pixel comparisons of the form

$$I_{q_1} \overset{?}{>} I_{q_2} \quad \text{for} \quad q_1, q_2 \in N(p) \tag{13.1}$$

Such a comparison provides a single-bit value of 0 or 1. For convenience of notation, we may rewrite the bit obtained as $\sigma(\beta^T I_{N(p)})$, where β is a $|N(p)|$-dimensional sparse vector, with two nonzero values, one equaling 1, the other equaling -1; and σ is the Heaviside function. For each fern m and pixel p, there are K bits computed, and we denote the kth bit as $b^m_{p,k} = \sigma((\beta^m_k)^T I_{N(p)})$. Collecting all the bits together, the K-dimensional bit vector b^m_p is:

$$b^m_p = \sigma\left(B^m I_{N(p)}\right) \in \{0, 1\}^K \tag{13.2}$$

where the matrix B^m has rows $(\beta^m_1)^T, \ldots, (\beta^m_K)^T$; and now the Heaviside function σ is applied element-wise.

Histogram of Bit Vectors We are interested in some translation invariance, so we take a spatial histogram over codewords. However, as in [24], the bit vectors *themselves* are the codewords; there is no need for an intermediate clustering step. Denote the histogram for the mth fern by $H^m(b)$, where bit vector $b \in \{0, 1\}^K$; then

$$H^m(b) = \sum_{p \in A^m} \delta\left(b^m_p - b\right) \tag{13.3}$$

where δ is a discrete delta function, and $A^m \subset \{1, .., P\}$ is the spatial aggregation region for fern m. Note that H^m is a sparse vector, with at most P nonzero entries.

Histograms concatenation The final decision is made by a linear classifier applied to the concatenation of the M fern histograms.

$$f(I) = W^T H(I) = \sum_{m=1}^{M} \sum_{b \in \{0,1\}^K} w^m_b H^m(b) \tag{13.4}$$

where $H(I) = [H^1(I), \ldots, H^M(I)] \in \mathbb{N}^{M2^K}$ and $W = [W^1, \ldots, W^M] \in \mathbb{R}^{M2^K}$ is a weight vector. Combining Steps 1–3 in the pipeline, we arrive at the discriminative ferns ensemble classifier:

$$f(I; \rho) = \sum_{m=1}^{M} \sum_{b \in \{0,1\}^K} w^m_b \sum_{p \in A^m} \delta\left(\sigma\left(B^m I_{N(p)}\right) - b\right) \tag{13.5}$$

with the parameters $\rho = \{W^m, B^m, A^m\}_{m=1}^M$.

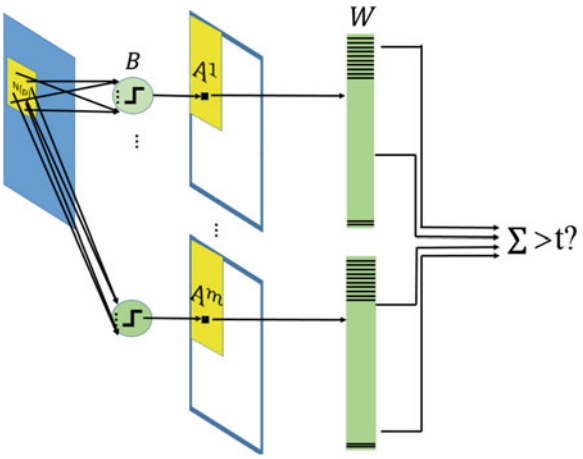

Fig. 13.1 A DFE network. A single fern in a DFE can be viewed as a feed-forward network with one highly non-linear layer and a second spatial summation layer. The DFE is a 3-layer network linearly aggregating the output of M ferns. See text for details

The operation of a DFE is sketched as a three-layered network in Fig. 13.1. Each fern can be conceived as a two-layer network. The first layer extracts a highly non-linear patch descriptor around each pixel p in the aggregation area. The patch descriptor is based on comparison of K pixel pairs, squashed into K bits, and concatenated into an single index. This index is then used to get a weight from the fern table. The operation is repeated for all pixels in the fern spatial aggregation area (the yellow rectangle in the second layer), and the contribution of all the pixels are summed. At a third layer, the contributions of all the ferns are linearly added and compared to a threshold to get the decision.

13.3.2 Classification Speed

Algorithm 1 describes the operation of a DFE classifier at test time. The pipeline is extremely simple. For each fern and each pixel in the fern's aggregation region, we compute the bit vector, considered as a codeword index. The fern table is then accessed with the computed index, and the obtained weight is added to the classification score. The complexity is $\mathrm{O}\left(M\overline{A}K\right)$ where $\overline{A}$ is the average number of pixels per aggregation region: $\overline{A} = \frac{1}{M}\sum_m |A^m|$.

It is interesting to compare the CPU time of a single fern to a single tree with the depth K. From a pure computational complexity perspective, the number of operations for both is K. Nevertheless, a closer look at their match to common CPU architectures, including cache hierarchies and vector machines, reveals large differences in expected run time. First, a tree needs to store the bit computation parameters for 2^K internal nodes. More importantly, during tree traversal, the working

Algorithm 1 Ferns Ensemble: Classification

Input: An image I of size $S_x \times S_y$,
classifier parameters $(B^m, A^m, W^m)_{m=1}^M$, threshold t
$B^m \in \mathbb{R}^{K \times |A^m|}$, $A^m \subset \{1, .., S_x\} \times \{1, .., S_y\}$, $W^m \in \mathbb{R}^{2^K}$
Output: A classifier decision in {0, 1}
Initialization: Score=0
For all ferns $m = 1, .., M$
    For all pixels $p \in A^m$
        Compute a k-bit index $= \sigma(B^m I_{N(p)})$
        Score=Score+W^m[index]
Return (Score>t)

set is accessed K times in an unpredictable manner. A fern's operation requires only a single access to its large working set (W^m), as the index computation is done using a small amount of memory, $O(K)$ in size, which fits in the cache without a problem.

Second, the usage of fixed pixel pairs in a fern enables computation of the K-bit index without indirection and with an unrolled loop. More importantly, ferns are amenable to vectorization using single-instruction multiple data (SIMD) operations, while trees are not. Applying a fern operation to several examples at the same time (i.e., vectorizing the loop over p in Algorithm 1) is straightforward. Doing so for a tree is likely to be extremely inefficient since each example requires a different sequence of memory accesses, and gathering such scattered data cannot be done in parallel in an SIMD framework. In Sect. 13.4.1.4, we further discuss the differences of ferns and random forest, in terms of classification time and memory.

13.3.3 Discriminative Training

The DFE classifier $f(I; \rho)$ is given in Eq. (13.5), and we would like to learn the parameters $\rho = \{W^m, B^m, A^m\}_{m=1}^M$ from a labeled training set $\{(I^i, y^i)\}_{i=1}^N$. Unlike prior work on ferns, e.g., [24], we turn to a discriminative rather than a generative formulation. In particular, we pose the problem as regularized hinge-loss minimization, similar to standard SVM:

$$\min_{\rho} \frac{1}{2}\|W\|^2 + C \sum_{i=1}^{N} \left[1 - y^i f\left(I^i; \rho\right)\right]_+ \tag{13.6}$$

where $[\cdot]_+$ indicates the hinge loss, i.e., $[z]_+ = \max\{z, 0\}$. Rewriting Eq. (13.4) with explicit parameter and image dependence one gets

$$f(I; \rho) = \sum_{m,b} w_b^m H^m \left(b, I \ ; B^m, A^m\right) \tag{13.7}$$

We can see that f is linear in W, so optimizing (13.6) w.r.t W for fixed $\{B^m, A^m\}_{m=1}^M$ is a standard SVM optimization. However, optimizing for the latter parameters is challenging, specifically since they are to be chosen from a large discrete set of possibilities. Hence, we turn to an agglomerative approach in which we greedily add ferns one at the time. As can be seen from Eq. (13.5), adding a single fern amounts to an addition of 2^K new features to the classifier. In order to do that in an sensible manner, we extend known results for the case of a single feature addition [2, 4].

Let $f(I) = \sum_{l=1}^{L-1} w_l x_l(I)$ be a linear classifier optimized with SVM and $L(f, \{I_i, y_i\}_{i=1}^N)$ the hinge loss obtained for it (Eq. 13.6) over a training set. Assume we add a single feature x^L to this classifier $f^{\text{new}}(I) = f^{\text{old}}(I) + w_L x^L(I)$, with small $|w_L| \leq \varepsilon$. Theorem 1 in [2] gives a linear approximation of the loss under these conditions:

$$L\left(f^{\text{new}}\right) = L\left(f^{\text{old}}\right) - w_L \sum_{i=1}^{N} \alpha_i y_i x_i^L + O\left(w_L^2\right) \tag{13.8}$$

where α_i are the example weights obtained as a solution to the dual SVM problem. The weights $\alpha_i \in [0, C]$ are only nonzero for support vectors. For a candidate feature x_L, the approximated loss (13.8) is best reduced by choosing $w_L = \varepsilon \cdot \text{sign}(\sum_{i=1}^N \alpha_i y_i x_i^L)$, and the reduction obtained is $R(x_L) \triangleq |\sum_{i=1}^N \alpha_i y_i x_i^L|$. The PFS algorithm [2] is based on training SVM using a small number of features, followed by computing the score $R(x)$ for a large number of unseen features; this allows one to add/replace existing features with promising feature candidates. Note that the score $R(x)$ of a feature column x can be seen as the correlation $R_Z(x) = x \cdot Z$, where $Z = (z_1, \ldots, z_n)$ with $z_i = y_i \alpha_i$ is the vector of signed example weights.

Here, we extend the aforementioned idea to a set of features, as introduced by a single fern. Assume we have trained an SVM classifier over a fern ensemble $f^{M-1}(I)$ with $M-1$ ferns, and we now wish to extend to an additional fern. Assume further that the new weight vector is small with $||w^m||_\infty \leq \varepsilon$. Then, we have

$$f^M(I) = f^{M-1}(I) + \varepsilon \sum_{b \in \{0,1\}^K} w_b^m H^m(b, I) \tag{13.9}$$

with $|w_b^m| \leq 1$ for all b. Treating the new fern contribution as a single feature, we can apply the theorem stated above and get

$$\begin{aligned} L\left(f^M(I)\right) &\approx L\left(f^{M-1}\right) - \varepsilon \sum_{i=1}^{N} \alpha_i y_i \sum_{b \in \{0,1\}^K} w_b^m H^m(b, I_i) \\ &= L\left(f^{M-1}\right) - \varepsilon \sum_{b \in \{0,1\}^K} w_b^m \sum_{i=1}^{N} \alpha_i y_i H^m(b, I_i) \end{aligned} \tag{13.10}$$

Algorithm 2 Ferns Ensemble: Training

Input: A labeled Training set $\{I_i, y_i\}_{i=1}^N$
Parameters $M, K, C, N_c, \{A^m\}_{m=1}^M$
Output: A classifier $(B^m, A^m, W^m)_{m=1}^M$, threshold t
Initialization: $Z[i] = 1/|\{I_i | y_i = 1\}|$ if $y_i = 1$,
$Z[i] = -1/|\{I_i | y_i = -1\}|$ if $y_i = -1$
For $m = 1, .., M$
For $k = 1, .., K$
For $c = 1, ..N_c$
Sample a candidate column $\beta_{k,c}^m \in R^{|N(p)|}$
For $i = 1, .., N$
Compute $H^m(b, I_i, c) = H^m(b, I_i; B_c^m)$
with $B_c^m = [\beta_1^m, .., \beta_{k-1}^m, \beta_{k,c}^m]$
For $b \in \{0, 1\}^K$
Compute $R_Z(c) = \sum_{b\in\{0,1\}^K} R_Z(H^m(b; \beta_{k,c}^m))$
Choose winning candidate $c^* = argmax_c R(c)$,
and set $\beta_k^m = \beta_{k,c^*}^m$
Train an SVM with $m2^K$ features $W \cdot [H^1, .., H^m] - t$
Set $Z[i] = y_i \alpha_i$ for $i = 1, .., N$ with α_i SVM dual variables
Set $\{W^m\}_{m=1}^M$, t based on the last SVM training.
Return $(B^m, A^m, W^m)_{m=1}^M$, threshold t.

where the approximation in the first equation is due to omission of $O(\varepsilon^2)$ terms. If we wish to minimize the approximated loss, the optimal choice for w_b^m is $w_b^m = \text{sign}(\sum_{i=1}^N \alpha_i y_i H_t^m(b, I_i))$, in an analogous way to the single feature case. With these w_b^m, we get

$$L\left(f^M(I)\right) \approx L\left(f^{M-1}\right) - \varepsilon \sum_{b\in\{0,1\}^K} R\left(H^m(b)\right) \tag{13.11}$$

This result is an intuitive extension of Theorem 1 in [2] for the case of multiple feature addition.

Our algorithm for fern ensemble growing is based on iterating between SVM training and building the next fern based on Eq. (13.11). This procedure is described more precisely in Algorithm 2. At each fern addition step, we use an SVM classifier trained on the previous ferns to get signed example weights, in a manner similar to boosting. The ensemble score $\sum_{b\in\{0,1\}^K} R_Z(H^m(b))$ is used to grow the fern bit by bit in a greedy fashion. At each bit addition stage, we randomly select N_c candidates for the mask β_k^m, termed $\beta_{k,c}^m$; each candidate is chosen by randomly drawing the two pixels needed for the comparison. The winning bit is chosen as the one producing the highest ensemble score. We currently do not optimize the integration area variables $\{A_m\}_{m=1}^M$, but we experiment with several choices in Sect. 13.4.

The algorithm is presented for a single binary problem, but is easily extended to training of several classes with shared A^m, B^m and separate W^m. In the simplest alternative independent SVMs are trained, one for each class of interest. During

optimization, all the SVMs are trained at each fern addition, and $R(c)$ scores of all of them are summed to make the bit choice. Due to the sharing of the same fern-based features, running time scales sublinearly in the number of classes. However, memory and training time are linear in the number of classes. For a large number of classes, error-correcting output codes [8] (ECOC) can be used to decrease the number of SVM classifiers trained, and enable a logarithmic scaling of training time and memory in the number of classes. In Sect. 13.4.2, we present experiments with this approach, showing that it enables economic classifiers with enhanced accuracy.

13.4 Empirical Results

The method described in this paper was developed, tested, and compared to alternatives on a very large data set for hand shape recognition. The task was discrimination between 3 hand state classes, and the resulting classifier was shipped as part of the Microsoft Xbox-1 console in early 2014. We describe these experiments in Sect. 13.4.1. In Sect. 13.4.2, we describe experiments conducted on a synthetically generated data set of 81 hand state classes. Scalability to a large number of classes is obtained by fern sharing and utilizing an error-correcting output codes (ECOC) approach.

13.4.1 Real Data Experiments

We describe the data set used in Sect. 13.4.1.1 and the method's implementation details in Sect. 13.4.1.2. The impact of the main ingredients and parameters of the method is tested in Sect. 13.4.1.3. We compare the accuracy–speed trade-off enabled by the proposed method and various competing techniques in Sect. 13.4.1.4. We conclude by showing the trade-offs between accuracy, classification time, training sample size, and memory in Sect. 13.4.1.5.

13.4.1.1 Data Set

The task we consider is to recognize three different hand shapes and to discriminate between them and other undefined hand states. The recognition results are used as part of a NUI interface. The shapes are termed 'open,' 'closed,' 'lasso,' and 'other,' as shown in Fig. 13.2. The class 'other' includes a large variation in hand poses, including hands holding objects. Hand detection is achieved by tracking the skeleton in a sequence of depth+IR images, using methods based on [25].

The images used for recognition are cropped around the extracted hand position, rotated, and scaled to two 36×36 images of the depth and IR channels. A simple preprocessing rejects IR and depth pixels where the depth is clearly far beyond the

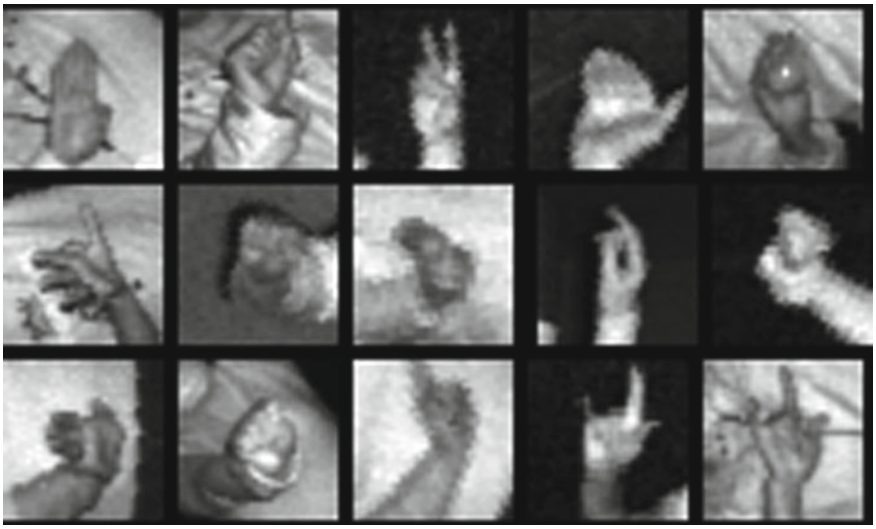

Fig. 13.2 Examples of hand images from our data set. The *left columns* contain examples of 'open,' 'closed,' and 'lasso,' respectively. The two *right columns* contain examples of the complement class 'other'

hand, thereby removing some of the background. The alignment and rotation of the hand are based on estimated wrist position and is sometimes inaccurate, making the recognition task harder.

A dataset of 519,000 images was collected and labeled from video sequences of different people. Images have considerable variability in terms of viewpoints, hand poses, distances, and imaging conditions. The images were taken at distances of up to $\sim$4 m from the camera, where the quality of image drops, and the depth measurement of fingers may be missing. Data were divided into training and test sets with 420,000 and 99,000 images, respectively, such that persons from the training set do not appear in test images and vice versa. The data were collected to give over-representation to hard cases. Given the properties of data, the goal was to achieve 2–5 % false-negative rate, at a false-positive rate of 2 %. Since the test data are hard, the error rate in real usage scenarios is expected to be much lower.

13.4.1.2 Implementation Details

In our experiments, we tested the number of bits per fern K in the range of [3, 18] and the number of ferns M in [6, 768]. At each bit addition step $N_c = 40$, pixel comparison features were randomly generated for evaluation. The spatial aggregation area of the fern A_m was randomly chosen to be one of the 4 standard quadrants of the image patch, and the neighborhood $N(p)$ is 17×17 pixels. We have experimented with limiting the aggregation area A_m further by imposing a virtual checkerboard

on the quadrant pixels: for odd bit indices, features are only computed for 'white' pixels, and for even indices, features are computed only for 'black' ones. This policy was found to be useful in terms of accuracy–speed trade-offs.

We have used the LibLinear package [14] for sparse SVM training of our models. The classifier was implemented in C and running times are reported on Intel core i7, 2.6 GHz CPU, using a single thread. Computation time is reported for a single image in milliseconds, without usage of SIMD optimizations. Accuracy of a single binary classifier, i.e., one hand pose versus all, is computed as the false-negative error rate at the working point providing a false-positive (FP) rate of 2 %. Accuracy figures reported here are averaged over the three classes. We selected this approach rather than multi-class error rate, as in each specific NUI usage context, the three classification scores are combined in a different way.

13.4.1.3 Parameters and Variations

Success and failure examples of the DFE classifier can be seen at Fig. 13.3. We now concentrate on understanding the contribution to performance of algorithm components.

Complexity of layers 1: At the first layer, we encode patches into codeword indices, and its complexity is controlled by the number of bits K used for the encoding. In Fig. 13.4 (Left), the classifier accuracy is plotted as a function of K for fixed $M = 50$. Based on this graph, we select the value of $K = 13$ in our subsequent experiments, as it is the minimal value which yet provide close to optimal accuracy.

Complexity of layers 2: At the second, spatial aggregation layer, complexity is controlled by several algorithmic choices. First, we can use multiple aggregation areas, or a single aggregation area containing the whole image for all ferns. Second, we can use or avoid using the checkerboard technique for computational saving. Results are reported in Fig. 13.5 (left). Baseline DFE uses $M = 50$ ferns with

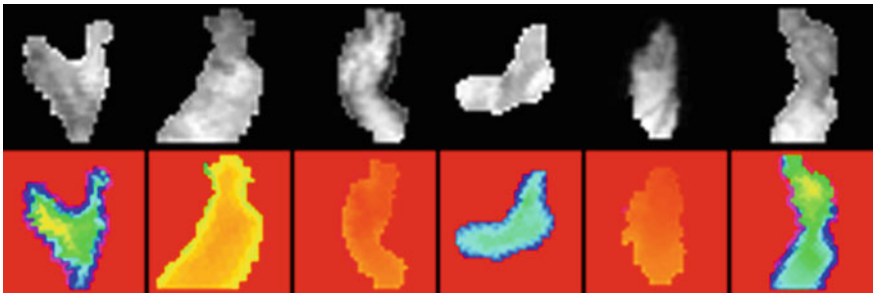

Fig. 13.3 Successes and failures of the DFE classifier: Pairs of depth+IR images are presented, where the *top row* shows the IR images and the *bottom* the depth images in every pair. The three pairs on the *left* show successfully classified pairs for the three hand shape classes considered (open, closed, lasso). The pairs on the *right* show misclassification errors (false negatives)

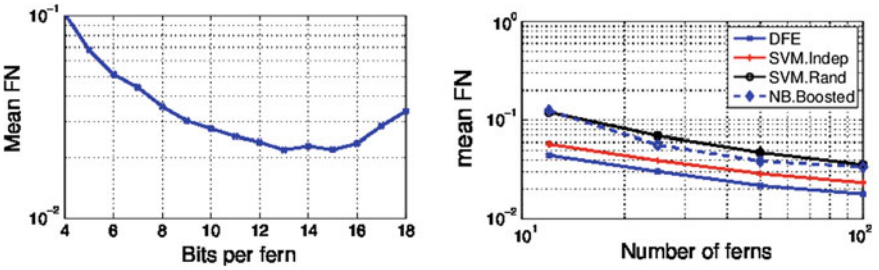

Fig. 13.4 DFE complexity parameters. *Left* False-negative rate of the DFE (at false-positive rate = 0.02 as a function of K, the number of bits. *Right* False-negative rate as a function of M, the number of ferns, for several training procedures. DFE is our baseline variation. For both SVM.Indep and SVM.Rand, SVM is used as final classifier. For SVM.Indep, the bits are selected using $R(c)$ score, but without PFS weight update, i.e., using initial $Z[i]$ for all ferns (see Algorithm 2). For SVM.Rand, bits are randomly selected. NB.Boosted is Naive Bayes with fern boosting and entropy-gain bit choice

Pipe variation	% FN @ FP=2%
Baseline DFE	2.18
Single aggregation area	3.15
No checkerboard sampling	2.42
Naive Bayes + Boosting	3.87
Naive Bayes, MI bits	35.9
Naive Bayes, Rand bits	47.6
Only Depth	4.65
Only IR	5.23

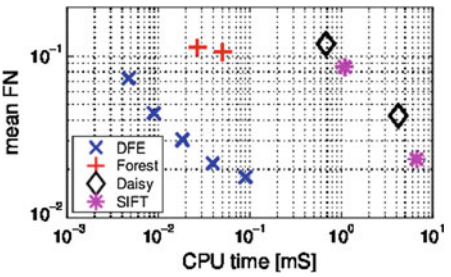

Fig. 13.5 Comparison to alternatives. *Left* Error for several DFE and Ferns algorithm variations. See text for explanation. *Right* Best results of false-negative rate under constraint of classification CPU time for various methods and parameters for each method. For DFE, we modified values of M, K. For random forest [17], the points shown are for one and two trees of depth 21. Fast SIFT can achieve accuracy comparable to DFE, but at cost of more than $\times 100$ classification time

quadrant ferns, checkerboard policy. The number of ferns used in the conditions 'single area' and 'no checkerboard' is reduced by a factor 4 and 2 to get classifiers with approximately the same speed as the baseline. The results show the advantage of baseline DFE over alternatives, hence led to its definition as 'baseline.'

Complexity of layer 3, optimization policy: Figure 13.5 (left) shows the accuracy for several ensemble training strategies. The simpler alternatives uses Naive Bayes, where the leaf weights are based on class posterior probabilities [6, 24]. The ferns are trained independently, with bits chosen at random (Naive Bayes, Rand bits) or by maximization of information gain (Naive Bayes, MI). For these alternatives, the false-negative rate is high. [2] Also, further increasing of the number ferns does not help

[2] Note that FN is measured at false-positive rate of 2 %. Hence, FN near 50 % is far better than random. At FP = 10 % the false-negative rates of Naive Bayes MI bits and Rand bits drops to 11 and 18 %, respectively.

as much as in the DFE or boosting framework, as the ferns are learned independently. Another alternative is training complementary ferns by boosting, with bits chosen to maximize the information gain on the boosting-reweighted sample (Naive Bayes + Boosting). This significantly improves accuracy relative to MI and random selection, but is still less accurate than DFE. Figure 13.4 (right) shows the effect of number of ferns, M, on the false-negative rate for selected methods.

From the above results, we can conclude that using discriminative (SVM) approach for both the final classifier and selecting of the fern bits significantly improves accuracy.

The table in Fig. 13.5 also shows that IR and depth are not redundant, and using both of them significantly improves accuracy relative to using only one of them.

13.4.1.4 Speed–Accuracy Trade-Off Comparison

We have compared the fern ensemble method to several alternative architectures, which also have an emphasis on a good speed-accuracy trade-off. The methods compared are:

- Random forest applied to pixel comparisons as suggested by [17]
- A 3-stages pipeline: (a) Fast dense SIFT features computation using the VLFeat library [28]. (b) Encoding into a bag of features using a random forest dictionary [23]. (c) SVM classification with a linear approximation of the histogram intersection kernel, according to [29]. We also tried the same pipeline, but replacing the fast SIFT with dense Daisy features [30].

All the methods were implemented in C/C++, using the original author's code when possible. They were chosen for comparison as each of them was developed with the aim of obtaining a good balance of speed and accuracy. Multiple working points were tested for each of these methods, representing various optimization for speed and accuracy. For the fast SIFT method, shifting between speed and accuracy was done by changing the stride parameter, controlling the density of the SIFT greed. For the Daisy, we also choose the Daisy complexity to optimize speed/accuracy, as recommended in [30].

The CPU time (accuracy) of the best working points obtained by each of the algorithms, including DFE, is plotted together in Fig. 13.6 (left). We see that random forest can achieve similar classification time to that of DFE, but is significantly less accurate (FN = 10.6 % vs. FN = 2 % for DFE, for the same CPU budget). Consistent with [17], we found that the best accuracy is achieved by training on a small number of deep trees, with little improvement when increasing the number of trees. This leaves us with less flexibility on controlling the trade-off between accuracy and classification time. There are several reasons why using 50 ferns DFE is about as fast as using two trees. First, each fern operates on relatively small number of pixels (50), which is only ∼4 % of the image. Second, calculating the ferns bits requires less operations than forest with the same depth, as discussed in Sect. 13.3.2. Third, the number of bit per fern is 13, while the depth of tree is 21. Also, the memory size

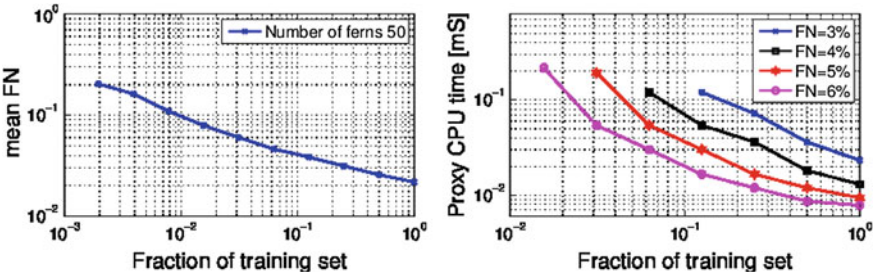

Fig. 13.6 *Middle* Accuracy obtained by DFE as a function of training sample size. X-axis is the fraction of training set size relative to the full set (420,000 images). *Right* The classification CPU time, as a function of training sample size. This is measured for several target false-negative rates (for a fixed FP = 2 %)

of the forest is in order of 80 MB versus 2.5 MB of ferns. Since 80 MB cannot fit into the cache, we pay with more cache misses.

The accuracy of with fast SIFT and Daisy alternatives can approach the accuracy of the DFE. However, their classification time is two order of magnitudes longer. By optimize them for speed, we significantly loose accuracy without getting to the target classification time.

In the next section, we show that in addition to high accuracy and fast classification, DFE approach enables significant flexibility for various trade-offs of speed, accuracy, memory size and generalization from various sizes of training set.

13.4.1.5 Training Sample Size and Memory

As discussed before, the fern ensemble architecture trades speed and accuracy for sample size and memory. For each training set size, constraints on memory, and classification time, we optimize accuracy by tuning M and K. In this section, we show that increasing the training set size enables us not only to improve accuracy, but also to significantly reduce the classification time.

Figure 13.6 (middle) shows the effect of increasing the training set size on FN, for fixed M and K. We modify the training set size we used from ∼0.2 % of the full set (820 images) to the full training set (420,000 images). The subset of training set is selected randomly. As expected, the false-negative rate reduces with increase of training set size.

In our problem, however, even with a training set size of ∼30,000 samples (0.07 in X-axis of Fig. 13.6), the accuracy we got met minimum requirements for the product. However, even after full code optimization, the classification time significantly exceeded the target budget. The question is if we can reduce classification time by increasing the training set size and modifying M and K.

Figure 13.6 (right) shows the classification time as a function of the of training set size, relative to the full set, for various target false-negative rates. We can see that for a fixed target accuracy, the classification time can be reduced by an order of

Table 13.1 Accuracy obtained by DFE under memory limits

LUT entries	Ferns # (M)	Bits # (K)	% FN @ FP = 2 %
768	48	4	10.7
1536	96	4	7.78
3072	96	5	6.07
6144	192	5	5.42
12288	384	5	4.21
24576	384	6	2.97
49152	768	6	2.32

LUT entries is the total number of entries in all the lookup tables (ferns) together, which is $2^K M$. In our implementation, each LUT entry requires 6 bytes—two bytes per class, representing the SVM weights

magnitude, if we increase the training set size by an order of magnitude. In general, as training set size increases, we slightly increase K and significantly reduce M to achieve same target accuracy with lower classification time. This can be explained by the effect of K on the capacity of each fern and hence should be adapted to the training set size. On the other hands, the accuracy can be improved by increasing M, but at a significant cost of classification time. These results are significant for building practical systems. While it is well known that increasing training set size enables improvement in accuracy, here, we show that it can also reduce classification time significantly.

Finally, we show the trade-off between memory and accuracy. Table 13.1 presents false-negative rate versus memory consumption for a fern ensemble. Memory consumption can be reduced by lowering either M or K, and in the table, we chose the optimal M, K parameters for each memory limit point. From the table, we can see adding a memory constraint leads to significant reduction in the number of bits per fern and increasing the number of ferns. The result is very different from the case of optimizing for classification time, where optimal number of bits is high. This is not surprising, as the memory size increases exponentially with number of bits, but classification time increases only linearly. The result classification time is about 5–10 larger when we optimize for memory instead of for speed. Note, however, that in our baseline implementation, with 50 ferns and 13 bits, the memory size is about 2.5 MB, which still fits into the cache.

13.4.2 Class Scalability Experiments

In this section, we show how a DFE can efficiently scale up to a large number of classes, while maintaining its beneficial accuracy and speed characteristics. Experiments are done using a synthetically generated dataset of 81 classes.

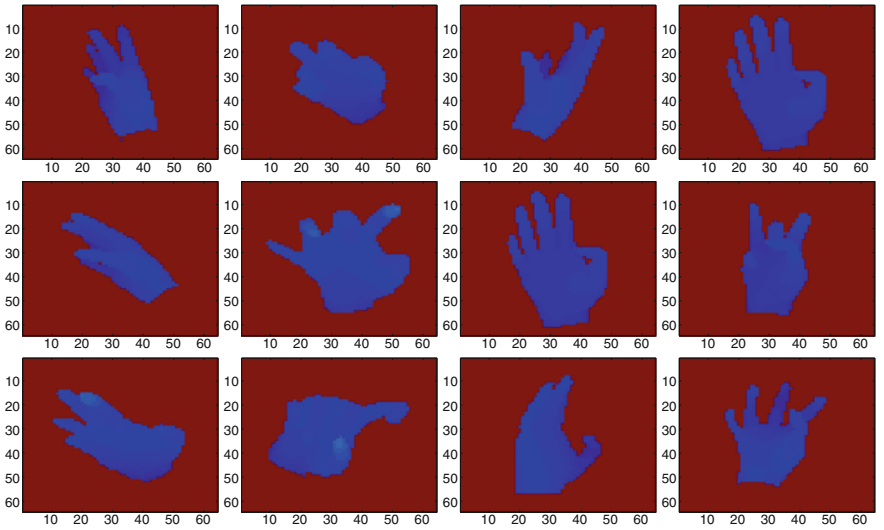

Fig. 13.7 Synthetic data for 81 classes. Hand state classes were generated by varying 4 independent variables: hand bend angle, twist angle, side angle, and pose. *Left Column* The bend angle was sampled uniformly in $[-30, 90]$ degrees, with 0 corresponding to a vertical hand. The range was split into 3 equal partitions to get the bend label of 1, 2 or 3, examples of which are given at rows 1, 2, 3, respectively. *Second column* The twist angle was sampled uniformly in $[-60, 60]$ degrees. Like the bend angle, it was quantized uniformly into 3 classes. *Third column* The side angle was sampled uniformly in $[-45, 45]$ degrees and quantized into 3 classes. *Right Column* 3 basic finger poses were considered: flat (*top*), half open (*middle*), and open (*bottom*). Independent finger noise was added to each finger's open/close parameter. The class label was set as a Cartesian product of the 4 base labels

13.4.2.1 Dataset and Parameters

We used POSER, a commercially available software package, for generating a dataset of hand pose depth images. A dataset of 62,317 examples was generated and randomly split into 37,390 training samples and 24,927 test samples. Data variance was controlled by varying 4 independent parameters of hand generation: the 3 rotation angles and the basic hand pose. Figure 13.7 shows examples from the dataset and explains its 4 dimensions of variability, as well as the labels that were given to the images. The 3 rotation angles (bend, twist and side) were uniformly sampled in ranges covering the viewing sphere of a frontal hand. The pose was generated by choosing a base pose from the set (flat hand, half-open hand, open hand) and adding a small amount of noise to the bend parameter of each finger independently. Each of the 4 dimensions was quantized into 3 different classes, and the final label is the combination of the 4 single-dimension labels.

The data included only depth images, 8 bits per pixel, and no attempt was made to synthesize IR images. In each image, the hand bounding box was found (the tightest

box containing all nonzero pixels), and the hand box was rescaled to 64×64 pixels images, which are the input of the DFE.

Preliminary experiments were done with 1/4 of the training set in order to choose DFE parameters and configuration. According to these experiments, we chose the pixel neighborhood $N(p)$ to be a large 32×32 patch. The integration area A_m was set to the internal 32×32 square of the 64×64 image. Checkerboard sampling was applied, but the use of quadrant ferns was not found to be superior; thus, we use the same integration area for all the ferns. The optimal number of bits was found to be 14.

13.4.2.2 Experiments

We have experimented with two variants of M-classification. The first is the basic one-vs-all, in which 81 SVMs are trained, one per class. As mentioned in Sect. 13.3.3, fern bits are chosen to optimize the sum of the gradient scores $R(c)$ of all the classes. A second alternative we tried was to solve for each of the label dimensions independently, i.e., we built 4 classifiers predicting the pose, bend angle, twist angle, and side angle of the hand. Each of these 4 classifiers, in turn, is composed of 3 one-vs-all SVMs, trained to separate one cell of the partition from the other 2 cells. Overall, in this approach, only 12 SVMs are trained, and the final label is determined based on the product code of the predicted 4 aspect labels.

Figure 13.8 (right) shows the multi-class accuracy obtained by both methods as a function of the number of ferns used. Both methods go beyond 80 %, which is quite high considering the large number of classes and the lack of margin in the boundaries between classes. Interestingly, the product code DFE, training only 12 classifiers, achieves higher accuracy than the one-versus-all version when the number of ferns is large (>10). Hence, in this domain, this version dominates the one-versus-all version in all respects, as it also provides higher speed in test and training, and requires less memory.

Method	Accuracy (%)	Speed (ms)	Memory (MB)
DFE 12SVM, 100 Ferns	84.5	4.87	38.5
DFE 81SVM, 100 Ferns	81.7	14.54	260
Forest 4Trees, D=18	70.3	12.62	179
Forest 1Tree, D=18	70.0	4.06	44
DFE 12SVM, 10 Ferns	80.0	0.52	3.9

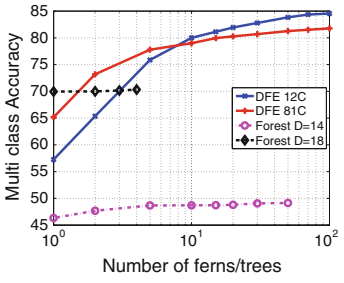

Fig. 13.8 Results for 81 classes. *Left* Multi-class accuracy, classifier speed, and model memory foot print of several hand classifiers. *Right* Accuracy as a function of the number of ferns/trees for DFE and Random forest classifiers

For comparison, we plot the accuracy obtained by a generatively trained forest, using code from [17]. When trees of depth 14 are used (matching our 14-bit ferns), performance is significantly inferior. The forest does better when its depth is not limited, and in this case, its maximal depth, limited by the dataset size, is 18. Forests of depth 18 are able to achieve 70 % accuracy, but their memory footprint is very large and becomes prohibitive for more than a few trees. We have experimented with up to 4 trees in this setting, and it seems that accuracy hardly improve with the number of trees.

In Table 13.1 (left), we compare the results obtained by the two DFE versions to the best results obtained by a classification forest [17] in terms of accuracy, speed, and memory. It can be seen that DFEs provide superior performance in each of the relevant measurements.

13.5 Conclusions and Further Work

We have seen that the *discriminative fern ensemble* framework enables significant push of the accuracy–speed envelope for visual recognition in IR+depth images. Thin, efficient architecture, and discriminative optimization were found important for this purpose. The method was shown to be scalable in the number of classes, thanks to feature sharing among classifiers and an ECOC methodology. In terms of architecture, it would be interesting to extend the table-based approach to deeper models with more table layers. Another interesting direction is to explore the trade-off between classification time and training sample size for other algorithms and analyze this trade-off theoretically.

References

1. Bar-Hillel A, Hanukaev D, Levi D (2011) Fusing visual and range imaging for object class recognition. In: IEEE international conference on computer vision (ICCV) 2011
2. Bar-Hillel A, Levi D, Krupka E, Goldberg C (2010) Part-based feature synthesis for human detection. In: Computer vision-ECCV 2010
3. Benenson R, Mathias M, Timofte R, Gool LJV (2012) Pedestrian detection at 100 frames per second. In: IEEE conference on computer vision and pattern recognition (CVPR) 2012
4. Bi J, Zhang T, Bennett K (2004) Column-generation boosting methods for mixture of kernels. In: Proceedings of the tenth ACM SIGKDD international conference on Knowledge discovery and data mining (KDD) 2004
5. Bo L, Lai K, Ren X, Fox D (2011) Object recognition with hierarchical kernel descriptors, In: IEEE conference on computer vision and pattern recognition (CVPR) 2011
6. Bosch A, Zisserman A, Muñoz X (2007) Image classification using random forests and ferns. In: IEEE international conference on computer vision (ICCV), pp 1–8
7. Dean T, Ruzon M, Segal M, Shlens J, Vijayanarasimhan S, Yagnik J (2013) Fast, accurate detection of 100,000 object classes on a single machine. In: Proceedings of IEEE conference on computer vision and pattern recognition, Washington, DC, USA, 2013

8. Dietterich TG, Bakiri G (1995) Solving multiclass learning problems via error-correcting output codes. J Artif Intell Res 2(1):263–286
9. Dietterich TG, Fisher D (2000) An experimental comparison of three methods for constructing ensembles of decision trees. Mach Learn, 139–157
10. Doliotis P, Athitsos V, Kosmopoulos DI, Perantonis SJ (2012) Hand shape and 3d pose estimation using depth data from a single cluttered frame. In: ISVC 2012
11. Dollár P, Belongie S, Perona P (2010) The fastest pedestrian detector in the west. BMVC, UK
12. Dollár P, Tu Z, Perona P, Belongie S (2009) Integral channel features. BMVC, UK
13. Erol A, Bebis G, Nicolescu M, Boyle RD, Twombly X (2007) Vision-based hand pose estimation: a review. Comput Vis Image Underst 108(1–2):52–73
14. Fan R, Chang K, Hsieh C, Wang X, Lin C (2008) Liblinear: a library for large linear classification. J Mach Learn Res 9:1871–1874
15. Han J, Shao L, Xu D, Shotton J (2013) Enhanced computer vision with microsoft kinect sensor: a review. In: IEEE transactions on cybernetics 2013
16. Keskin C, Kirac F, Kara Y, Akarun L (2011) Real-time hand pose estimation using depth sensors. In: IEEE international conference on computer vision (ICCV) 2011
17. Keskin C, Kirac F, Kara YE, Akarun L (2012) Hand pose estimation and hand shape classification using multi-layered randomized decision forests. In: Computer vision-ECCV 2012
18. Lazebnik S, Schmid C, Ponce J (2006) Beyond bags of features: spatial pyramid matching for recognizing natural scene categories. In: IEEE Computer Society conference on computer vision and pattern recognition (CVPR) 2006
19. Levi D, Silberstein S, Bar-Hillel A (2013) Fast multiple-part based object detection using kd-ferns. In: IEEE Computer Society conference on computer vision and pattern recognition (CVPR)
20. Liu L, Shao L (2013) Learning discriminative representations from RGB-D video data. In: Proceedings of the twenty-third international joint conference on artificial Intelligence (IJCAI) 2013
21. Lowe DG (2004) Distinctive image features from scale-invariant keypoints. Int J Comput Vis 60(2):91–110
22. Mason L, Baxter J, Bartlett P, Frean M (2000) Boosting algorithms as gradient descent. NIPS
23. Moosmann F, Triggs B, Jurie F (2007) Fast discriminative visual codebooks using randomized clustering forests. Adv Neural Inf Process Syst
24. Ozuysal M, Calonder M, Lepetit V, Fua P (2010) Fast keypoint recognition using random ferns. IEEE Trans Pattern Anal Mach Intell 32(3):448–461
25. Shotton J, Sharp T, Kipman A, Fitzgibbon AW, Finocchio M, Blake A, Cook M, Moore R (2013) Real-time human pose recognition in parts from single depth images. Commun ACM 56(1):116–124
26. Tang D, Yu T, Kim T-K (2013) Real-time articulated hand pose estimation using semi-supervised transductive regression forests. In: International conference on computer vision (ICCV) 2013
27. Tola E, Lepetit V, Fua P (2008) A Fast Local Descriptor for Dense Matching. In: IEEE conference on computer vision and pattern recognition (CVPR) 2008
28. Vedaldi A, Fulkerson B (2008) VLFeat: an open and portable library of computer vision algorithms. http://www.vlfeat.org/
29. Vedaldi A, Zisserman A (2011) Efficient additive kernels via explicit feature maps. Pattern Anal Mach Intell 34(3)
30. Winder S, Hua G, Brown M (2009) Picking the best daisy. In: IEEE conference on computer vision and pattern recognition (CVPR)